Super-Hydrophobic Surfaces via Micrometer-Scale Templated Pillars

Nicole E. Zander,[†] Joshua A. Orlicki,[†] Afia S. Karikari,[‡] Timothy E. Long,[‡] and Adam M. Rawlett*,[†]

United States Army Research Laboratory, Aberdeen Proving Ground, Maryland 21005, and Department of Chemistry, Macromolecules and Interfaces Institute, Virginia Polytechnic Institute and State University, Blacksburg, Virginia 24061

Received June 14, 2007. Revised Manuscript Received September 11, 2007

The fabrication of enhanced hydrophobic surfaces via simple and inexpensive means will be discussed. Regular arrays of microscale pores were prepared in polymer matrices via the spontaneous assembly of water-vapor condensation, the so-called breath figure method. Using these regular arrays of pores as templates, the analogous array of pillars (inverse pores) was transferred to polymeric films. These microtextured surfaces have greatly enhanced the hydrophobicity of the polymer when measured by the contact angle. This method of producing super-hydrophobic textured surfaces should be amenable to high-throughput, low-cost manufacturing of many polymeric surfaces.

1. Introduction

The formation of hierarchically ordered arrays of spherical cavities on polymer films is of interest because of potential applications in the preparation of photonic bandgap materials, environmental sensors, and patterned light-emitting diodes (LEDs).[1–5] While many methods are known for the preparation of these porous materials, the breath figure approach has received significant examination because of the simple and robust mechanism of pattern formation.[4,6] Breath figures are patterned arrays of micrometer-sized defects in a polymer film, formed when water droplets condense onto a polymer solution surface during film drying. When variables such as relative humidity and polymer concentration are controlled, the feature size and uniformity of the resultant pattern can be controlled.[7,8]

The process is driven by the evaporation of the solvent under humid conditions, leading to a decrease in temperature at the air–liquid interface. The resulting water condensation[1] proceeds in several steps, beginning with the nucleation of droplets in random positions. As the droplets grow in size and number, they coalesce, adopting a regular pattern because of the thermodynamics of liquid–liquid surface energy minimization. With properly controlled conditions, free-energy minimization drives the subsequent ordering of the droplets into a hexagonal lattice.[9] The temperature difference between the solution surface and the ambient conditions diminishes as the surface of the film is uniformly covered by water droplets. At this stage, the water droplets may sink into the solution (depending upon solution density). Upon complete evaporation of the solvent, the pattern of the droplets generated in the polymer matrix is preserved as a hexagonally ordered array of pores with a honeycomb structure.[10,11]

Along with the desirability of ordered films for electronic applications, there is an ever-increasing appeal for ultra-hydrophobic, self-cleaning surfaces.[12] Materials with the lowest surface energies and smooth surfaces can only achieve contact angles of ca. 120°.[12–14] Wenzel, Cassie, and Baxter determined that the wettability of a surface is governed by both the surface energy and roughness.[12] According to Wenzel's equation, roughness decreases wettability for low-energy hydrophobic surfaces but increases wettability for hydrophilic surfaces.[15] The Cassie–Baxter law describes the effective contact angle for a liquid drop on a composite surface. A very rough low-energy polymer surface increases the surface composition fraction of air and increases hydrophobicity.[16] The ultra-hydrophobicity of biological surfaces, such as the lotus leaf and the lady's mantle, has attracted a

* To whom correspondence should be addressed. Fax: 410-306-0676. E-mail: arawlett@arl.army.mil.
[†] Aberdeen Proving Ground.
[‡] Virginia Polytechnic Institute and State University.

(1) Böker, A.; Lin, Y.; Chiapperini, K.; Horowitz, R.; Thompson, M.; Carreon, V.; Xu, T.; Abetz, C.; Skaff, H.; Dinsmore, A.; Emrick, T.; Russell, T. *Nat. Mater.* **2004**, *3* (5), 302.
(2) Park, M.; Kim, J. *Langmuir* **2004**, *20* (13), 5347.
(3) Yabu, H.; Tanaka, M.; Ijiro, K.; Shimomura, M. *Langmuir* **2003**, *19* (15), 6297.
(4) Yabu, H.; Shimomura, M. *Langmuir* **2005**, *21* (5), 1709.
(5) Karikari, A.; Williams, S.; Heisey, C.; Rawlett, A.; Long, T. *Langmuir* **2006**, *22* (23), 9687.
(6) Englert, B. C.; Scholz, S.; Leech, P. J.; Srinivasarao, M.; Bunz, U. H. F. *Chem.—Eur. J.* **2005**, *11* (3), 995.
(7) Peng, J.; Han, Y.; Yang, Y.; Li, B. *Polymer* **2004**, *45* (2), 447.
(8) Barrow, M.; Jones, R.; Park, J.; Srinivasarao, M.; Williams, P.; Wright, C. *Spectroscopy* **2004**, *18* (4), 577.
(9) Marcos-Martin, M.; Beysens, D.; Bouchaud, J. P.; Godreche, C.; Yekutieli, I. *Physica A* **1995**, *214*, 396.
(10) Park, M. S.; Kim, K. K. *Langmuir* **2004**, *20*, 5347.
(11) Mohan, S.; Collings, D.; Phillips, A.; Patel, S. *Science* **2001**, *292*, 79.
(12) Luzinov, I.; Brown, P.; Chumanov, G.; Minko, S. http://mse.clemson.edu/htm/research/ntc/Ultrahydrophobic%20Fibers_1.pdf.
(13) Barthlott, W.; Neinhuis, C. *Planta* **1997**, *202* (1), 1.
(14) Otten, A.; Herminghaus, S. *Langmuir* **2004**, *20* (6), 2405.
(15) Wenzel, R. *Ind. Eng. Chem.* **1936**, *28* (8), 988.
(16) Cassie, A.; Baxter, S. *Trans. Faraday Soc.* **1944**, *40*, 546.

10.1021/cm0715895 CCC: $37.00
Published on Web 11/08/2007

great deal of attention.[17,18] These macroscopically smooth, microscopically rough, high aspect ratio surfaces can achieve contact angles upward of 160°.[17,19] High aspect ratios of some of these textured surfaces achieve a low hysteresis between advancing and receding contact angles, allowing for droplet motion.[20] Droplet movement generates a self-cleaning surface by removing dirt and grime as the droplet rolls.[12]

The fabrication of hydrophobic surfaces may also be achieved through a variety of mechanisms, such as fluoroplasma treatment of lithographically formed silicone pillars, grafting to or polymerization from a surface with fluorinated polymers, plasma etching, or chemical vapor deposition.[20] In addition, researchers at Clemson have fabricated a pillar-like surface out of a low surface energy triblock copolymer polystyrene-*b*-(ethylene-cobutylene)-*b*-styrene (SEBS), adding nanoparticles to increase the surface roughness.[21] Besides the costly but well-organized surfaces fabricated by lithographic methods, most of the aforementioned surface treatment techniques generate randomly ordered surfaces.[20] Furthermore, Herminghaus postulated that hierarchical roughness of similar ordering to naturally occurring fractal patterns could render any low-energy surface nonwettable with the contact angle potentially near 175°.[22,23] This paper discusses a novel application of the breath figure method in which the inexpensively generated ordered arrays are used as templates to construct pillars (inverse pores). These macroscopically smooth, microscopically rough surfaces improve the hydrophobicity of the polymer over 30° when compared to the smooth substrate.

2. Experimental Section

Materials. For breath figure pore formation, polystyrene (PS) with a series of molecular weights (M_n = 10, 19.8, 51, 97.1, 160, 411, and 670 kDa; polydispersity index (PDI) = 1.06 for all of the polymers) were purchased from the Pressure Chemical Company in Pittsburgh, PA. Monocarboxy- and dicarboxy-terminated PSs (M_w = 100 kDa) were purchased from Scientific Polymer Products.

To prepare the array of pillars, two different silicone rubbers were evaluated. A high viscosity, opaque rubber was obtained from Dow Corning 3120 RTV Silicone Rubber; GE Silicones provided a clear, low-viscosity resin, RTV615.

Atomic force microscopy (AFM) images were obtained on a Dimension 3100 AFM equipped with a Nanoscope IV scanning probe microscope controller. Laser-scanning confocal micrographs were taken with a Zeiss Pascal 5 confocal microscope equipped with two helium lasers and a multiwavelength argon laser. Optical images were obtained from a Leica DM/LP microscope.

Procedure. *Breath Figure Formation.* Two methods were used to form the highly ordered microscale arrays, i.e., breath figures. In the first setup, a humidity chamber was created using a plastic desiccator with a nitrogen inlet and a vent. To achieve a relative humidity of 65–80%, a saturated sodium chloride salt solution covered with parafilm wrap was placed in the chamber at ambient temperature. Nitrogen gas was bubbled through the saturated salt solution at a controlled rate. The relative humidity was measured with a digital Dickson hygrometer and could be controlled by changing the gas velocity. In the second setup, a Carson Environmental Chamber was used to electronically set the relative humidity, with the temperature kept near ambient conditions. The polymer solutions (1.0–10.0 wt %) were prepared by weighing the required amount of PS into a sample vial and dissolving it in dry CH_2Cl_2. Two different substrates were used and prepared as follows: Dupont Kapton polyimide film (thickness of 127 μm) was cut to the required size, rinsed twice with ethanol, and dried with nitrogen. The film was then ozone-treated for 20 s and taped to a standard glass microscope slide.

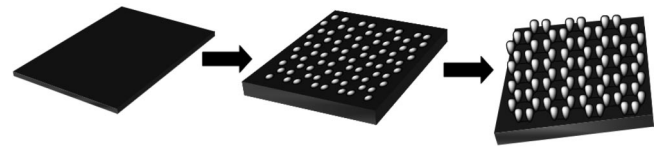

Figure 1. Schematic of the breath figure and pillar formation.

Glass microscope slides were also used as substrates to form the breath figures, but because of wettability issues, these substrates were first treated with a silane solution to make the surface more energetically compatible with the polystryrene. To modify the surface, the slides were passed through a flame to burn off any contaminants and then soaked for 1 h in a 1% propyltrimethoxy silane solution in 90% (v/v) ethanol and water solution with a pH of 4.5. After the slides were rinsed with ethanol, they were dried at 70 °C to complete the silane condensation.

After preparation, the appropriate substrates were placed in the humidity chambers and allowed a set time interval to equilibrate in the environment. An aliquot of the appropriate PS solution was then placed on the substrate in the humidity-controlled chamber, and the solvent was allowed to evaporate at a chosen temperature and humidity.

Pillar Formation. Using the aforementioned synthesized films as substrates, the PS template was covered with a degassed two-part silicone rubber formulation. This was cured ca. 18 h at 60 °C and separated from the PS (see Figure 1). Two methods were used to separate the pillars from the breath figure template. The two films were either mechanically peeled apart or the breath figure template was dissolved with an appropriate organic solvent. The silicone film was then removed, allowed to air-dry, and characterized by AFM and goniometry.

3. Results and Discussion

Breath Figure Formation. PS solutions of varied molecular weight were dissolved in dichloromethane and cast in a controlled humidity chamber. The surface of the polymer solutions subsequently became opaque, indicating the breath figure formation. Figure 2 shows the optical micrographs of four of the breath figure films generated at 62% relative humidity. The surface morphology of the films was significantly different, confirming the molecular weight as a key parameter influencing pattern formation. In particular, the solution viscosity, which varies with the molecular weight of the polymer, can be correlated to pore dimensions at a constant relative humidity. The lowest molecular-weight PS generated films with large defect pores spread throughout the film and small domains of uninterrupted ordering with

(17) Mock, U.; Förster, R.; Menz, W.; Rühe, J. *J. Phys: Condens. Matter* **2005**, *17*, S639.
(18) Feng, L.; Li, S. H.; Li, Y. S.; Li, H. J.; Zhang, L.; Zhai, J.; Song, Y.; Liu, B.; Jiang, L.; Zhu, D. *Adv. Mater.* **2002**, *14* (24), 1857.
(19) Northen, M.; Turner, K. *Nanotechnology* **2005**, *16*, 1159.
(20) Blossey, R. *Nat. Mater.* **2003**, *2* (5), 301.
(21) Herminghaus, S. *Europhys. Lett.* **2000**, *52* (2), 165.
(22) Kim, S. D.; Boczar, E. M.; Klein, A. *Langmuir* **2000**, *16*, 1279.
(23) Kim, S. D.; Klein, A.; Sperling, L. H.; Boczar, E. M.; Bauer, B. J. *Macromolecules* **2000**, *33*, 8334.

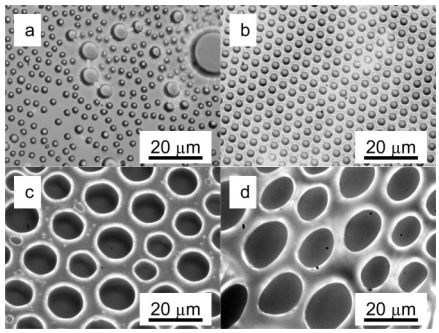

Figure 2. Optical micrographs of variable molecular-weight PS breath figures formed in CH_2Cl_2 (1 wt %) at 62% relative humidity: (a) 19.8, (b) 97.1, (c) 411, and (d) 670 kDa PS.

less than 0.7 μm variation between pore sizes. The solution viscosity of the 19.8 kDa solution may be too low to prevent neighboring water droplets from coalescing upon breath figure formation, producing the large pores which interrupted the long-range ordering. The 411 and 670 kDa solutions show a marked increase in pore size when compared to the 19.8–160 kDa films. The high viscosity of these solutions may interfere with the ability of the droplets to fully organize on the polymer surface, generating larger pores and also more variation between pores with standard deviations up to 4 μm. Optimal pore formation, under these conditions, was obtained with the 97.1 kDa PS, with standard deviations between pores less than 0.4 μm.

Although local ordering was achieved with some of the standard PSs examined, the areas of ordering with uniform pore size and spacing was limited to small domains and reproducibility of the films was inadequate. End-functionalized PSs were examined to ascertain if superior long-range ordering could be achieved. Of all the PSs examined, the dicarboxy-terminated PSs generated the most reproducibly ordered templates, with an average pore diameter and depth of 2.9 $\pm$ 0.2 and 0.91 $\pm$ 0.6 μm, respectively. Figure 3 displays optical micrographs of a dicarboxy-terminated PS film at a series of magnifications, illustrating the superb organization of the pores over millimeter-sized areas. Figure 4 contrasts the Fourier transform of carboxy terminated with a nonfunctionalized PS film. Although near-perfect hexagonal ordering is achieved with the monocarboxylated PS, better long-range ordering was seen in the dicarboxy-terminated PS.

The improved organization of the 100 kDa dicarboxy-terminated PS film compared to the 97.1 kDa PS, formed at identical conditions with similar solution viscosity, indicates that polymer functional groups could play a role in the regularity of the templated pattern. Enhanced arrangement of the pores in the carboxy-terminated PS over nonfunctionalized PS may be attributed to the effects of the end groups on the surface energy and aggregation of polymer chains. Ordinarily, the high surface energy carboxyl groups are absent at the air–polymer interface.[22] The onset of water droplet condensation during the breath figure formation process should drive the polar carboxyl end groups to the surface. Aggregation of the end groups because of hydrogen bonding leads to an effective increase in polymer molecular weight. The aggregation may contribute to stabilizing forces between the polymer and the water droplet, allowing for superior ordering over larger areas in comparison to the nonfunctionalized PS. Researchers from Lehigh found that disulfonated polymers achieved nearly 3 times the effective molecular weight compared to monosulfonated PSs when measured by GPC.[23] This research suggests that a similar correlation could be drawn for the carboxy-terminated PSs, possibly elucidating the superior long-range ordering of the dicarboxy-terminated PS over the monoterminated polymer. Other pertinent differences, which may have brought about improved pore organization for the carboxy-terminated PS, although not examined in this study, could be the interaction of the polymer with the water droplets or propyl-silane-treated substrate.

Templating from Breath Figures. To overcome some of the limitations inherent with PS, such as susceptibility to solvents and fragility, a more permanent pattern was sought. Silicone rubber proved a good choice because of its hydrophobic and durable nature. Thus, the pattern from the PS template was transferred to the rubber, generating silicone pillars. These pillars were obtained by coating breath-figure-derived films with silicone rubber, cross-linking the rubber, and then removing the PS template. Separation of the two polymers was achieved by dissolving the PS in tetrahydrofuran (THF) or mechanically peeling apart the polymers. Mechanical separation was nearly impossible for the carboxy-terminated PS, because of strong adhesion between the two polymers. The standard PSs easily separated from the low-viscosity silicone but adhered to the high-viscosity silicone. Figure 5 displays the breath figure template and resulting pillared surface formed in a controlled environment from the low-viscosity silicone rubber. The average pore diameter and depth were 4.4 $\pm$ 0.1 and 3.0 $\pm$ 0.3 μm, respectively. Conversely, the corresponding pillar diameter and depth (Figure 5c) were 10.6 $\pm$ 0.3 and 3.7 $\pm$ 0.4 μm, respectively. The increase in the pore dimensions may be attributed to swelling of the cross-linked pillars as a result of the residual solvent entrapped in the polymer matrix. Mechanical separation of the template and pillars yielded a much smaller increase in pillar diameter from 3.4 $\pm$ 0.1 to 4.5 $\pm$ 0.2 μm. Similar results were obtained for the pillars formed with the highly viscous silicone rubber, although the degree of the swelling was reduced. Reduced swelling of the high-viscosity silicone was expected because the cross-link density is greater than the low-viscosity silicone. The average pore diameter and depth for the 100 kDa dicarboxy-terminated PS were 2.91 $\pm$ 0.2 and 0.91 $\pm$ 0.6 μm, respectively, while the solvent-separated pillar diameter and height were 4.20 $\pm$ 0.4 and 0.83 $\pm$ 0.1 μm, respectively. On average, the pillar diameter was 45% larger when compared to the pore diameter for the high-viscosity rubber, while the pillar height was nearly identical to the pore depth. Mechanical separation was also attempted for these films but yielded mixed results, because the pillar surface was frequently damaged.

Contact angles were measured in several locations on the pillared surface using goniometry. Figure 6 demonstrates a linear relationship between the pore diameter and contact angle for high-viscosity silicone pillars formed from a series of templates of linear PS standards of varying molecular

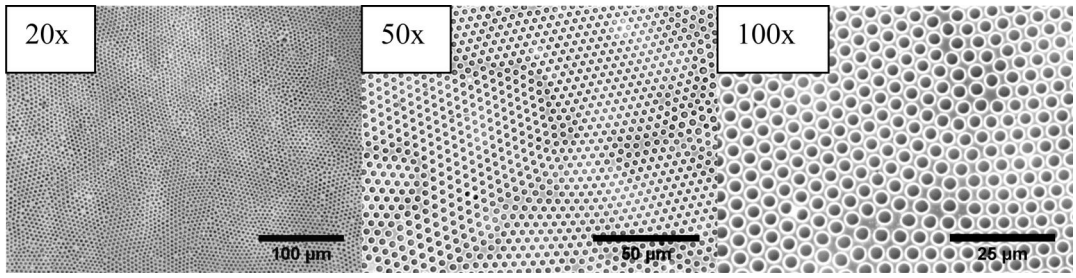

Figure 3. Series of optical micrographs of 1 wt % dicarboxy-terminated PS breath figures demonstrate the long-range ordering of the film.

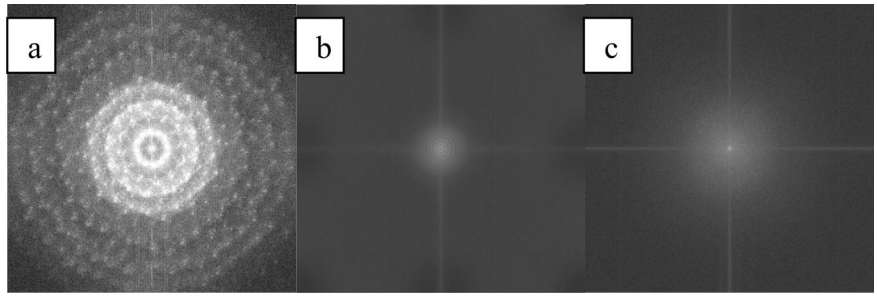

Figure 4. Fourier transform of (a) monocarboxy-terminated PS, (b) dicarboxy-terminated PS, and (c) nonfunctionalized PS.

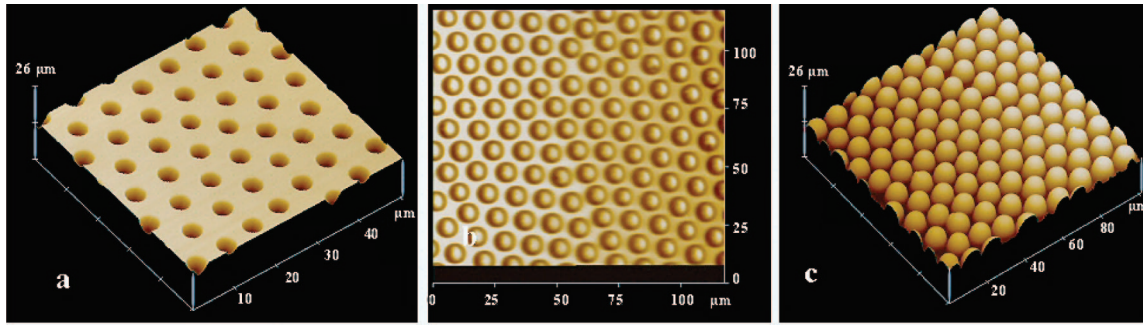

Figure 5. AFM images of silicone pillars (GE Silicons RTV 615 silicon rubber). (a) Breath figure template before templating step, (b) optical micrograph of the pillars, and (c) atomic force micrograph of the pillars.

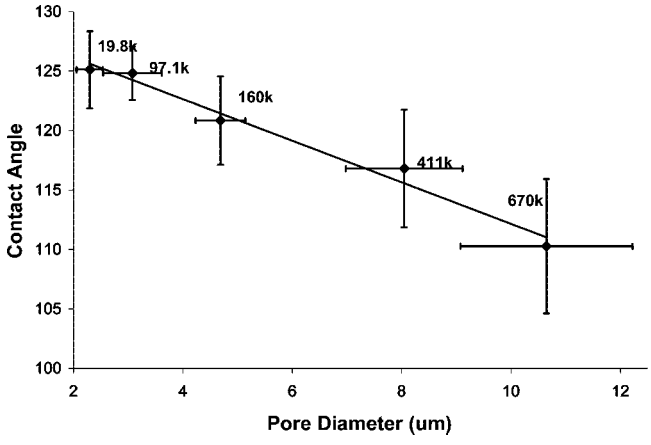

Figure 6. Series of linear PSs (M_w = 19.9–670 kDa) at 1 wt % and 62% relative humidity demonstrate that the contact angle is found to linearly decrease with an increasing pore diameter.

weights. Because the pillar height did not vary significantly between different molecular-weight templates, the smaller pore sizes (obtained from the lower molecular-weight PSs) achieved superior contact angles as a result of their higher aspect ratios. This relationship demonstrates an ability to predict or manipulate the wetting of a surface by changing the processing conditions or materials. As previously discussed, the feature size and spacing can be easily modified by varying the relative humidity or viscosity of the polymer solution.

The pillars prepared from the 2 wt % dicarboxy-terminated films with the viscous silicone yielded average advancing and receding contact angles of 136 ± 4° and 124 ± 4°, respectively, with the highest contact angle of 142°. Although the monocarboxy-terminated PS appeared to have superior regional organization (Figure 4), the areas of long-range ordering were significantly smaller. Thus, pillars were not fabricated using the former PS as a template.

To verify that ordered as opposed to random roughness yields more hydrophobic surfaces, unorganized pillars were made from disordered PS templates. These templates were prepared with conditions unsuitable for regular droplet packing, typically at relative humidities either above 90% or below 45%. Figure 7 depicts pillars formed by coating silicone rubber on disordered (Figure 7a) and ordered (Figure 7b) breath figure templates. The average diameter of the ordered array of pillars (Figure 7b) was 4.5 ± 0.2 μm, with a height of about 1.0 μm. Variation in the contact angle between ordered and disordered surfaces as measured by goniometry was approximately 30°, because the disordered

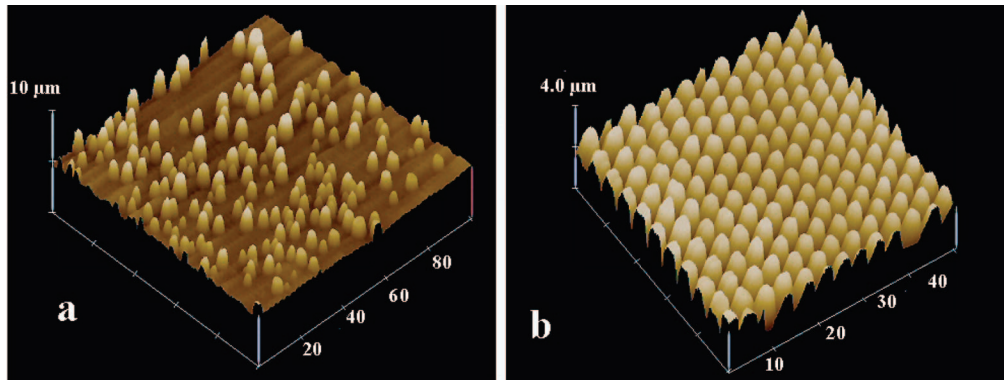

Figure 7. Three-dimensional AFM images of silicone pillars formed on breath figure templates. In a, the silicone rubber was cross-linked on a 51 kDa breath figure film formed in an uncontrolled environment, while b was cross-linked on a film of the same molecular weight formed in a humidity chamber at 73% relative humidity.

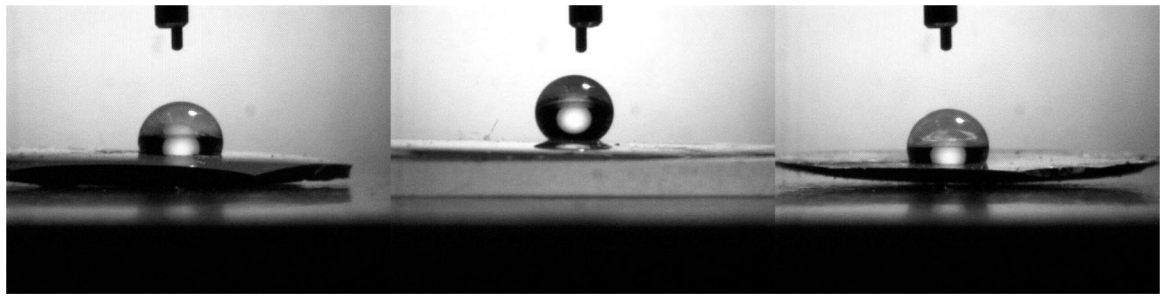

Figure 8. Contact angle measurement (goniometer). (Left) Cured Si rubber (control) advancing contact angle = 104°, and receding = 100°. (Middle) Cured Si rubber with pillars contact angle = 138°, and receding = 126°. (Right) Cured Si rubber with disordered pillars contact angle = 112°, and receding = 95°.

template yielded films with contact angles identical to the control. Thus, ordered microscopic roughness in our polymeric system influences hydrophobicity.

Figure 8 demonstrates the effect of micropatterning through breath figure templating on polymer surface morphology. Similar to the lotus leaf, micrometer roughness greatly enhances surface roughness, leading to a large increase in the hydrophobicity of a polymer surface.[17] The left image displays a water droplet on a smooth silicone surface, in which hydrophobicity is dictated almost entirely by the surface energy of the polymer. The middle image displays the same silicone surface roughed by ordered pillars. The greatly enhanced hydrophobicity demonstrates the necessity of surface roughness to achieve high contact angles. Finally, the right image depicts a water droplet on a disordered pillared surface. The hierarchically ordered surface obtains a significant increase in contact angle and only a moderate decrease in hysteresis over the disordered film, again indicating the superiority of organized roughness over random ordering.

4. Conclusion

Breath figure templating is a facile and robust method to manufacture hierarchically ordered hydrophobic surfaces. The hydrophobicity of the surface can be tuned by template modification achieved through alteration of the molecular weight, weight percent of the polymer, or the relative humidity of the casting chamber. The microscopically textured pillars enhance the hydrophobicity of the silicone by ca. 30–35° up to 142° when measured by the contact angle. In comparison to Teflon, a hydrophobic standard with a contact angle of 115°, silicone pillared surfaces show greater than 20% improvement via facile means. This method of producing hydrophobic surfaces provides a low-cost alternative to traditional fabrication techniques.

Acknowledgment. We thank ARO MAP MURI (DAAD19-02-1-0275) for funding and Mr. Donovan Harris and Dr. Mark VanLandingham for their assistance with optical characterization and atomic force microscopy.

CM0715895